PERFORMANCE IMPROVEMENT OF AN AXIAL FLOW COMPRESSOR

S.M. Swamy

Asst. Professor, G. Narayanamma Institute of Technology and Sciences, Shaikpet, Hyderabad, India.

ABSTRACT: The present paper reports results of an experimental investigation aimed at improving the performance and operating range of an axial flow compressor using a simple passive means. A total of four configurations are tested, namely, (i) basic rotor configuration without any passive means, (ii) rotor with partial shroud (PS), (iii) rotor with PS and turbulence generator, TG placed on the casing at the leading edge of the rotor blade and (iv) rotor with PS and turbulence generator, TG1, placed on the casing at 44 mm upstream of the leading edge of the rotor blade. The turbulence generators are made of velcro tape. The rotor performance is determined by measuring static pressure on the casing, upstream and downstream of the rotor blade. In addition, five hole probe traverses are made at the rotor exit at five flow coefficients (at, above and below design flow coefficients). From the casing static pressure measurements, stall flow coefficient of rotor (with PS + TG1) is found to be decreased. From the five hole probe measurements, rotor (with PS + TG1) is found to have improved total and static pressure coefficients compared to rotor (with PS). Slightly reduced performance of this rotor compared to the basic configuration is attributed to the adverse effects of PS. The improved performance of the rotor (with PS + TG1) is attributed to the energization of the casing wall boundary layer at the rotor inlet, due to vortexes generated by TG1.

Keywords: Compressor, Rotor with Partial Shroud, Rotor with PS &TG, Turbulence Generator Placed on the Casing.

Nomenclature

d	diameter, m
h	rotor blade chord, mm
PS	partial shrouds
n	impeller rotational speed, rpm
p	pressure, N/m^2
r	radius, m
s	blade spacing, mm
SS	suction surface
t	tip clearance, mm
TG	turbulence generator placed at the rotorleading edge
TG1	turbulence generator placed upstream the rotor leading edge
U	peripheral velocity, m/s
V	volume flow rate, m
τ	tip clearance as percentage of chord, $t/Ch_t \times 100$

Subscripts

1	rotor inlet
2	rotor exit
3	stator exit
b	blade
c	casing
h	hub
o	total
R	rotor
S	stator
s	static
t	tip

1. INTRODUCTION

Axial flow compressors have a wide range of applications especially for power plants and industrial applications compared to centrifugal compressors. Due to bulky construction, large frontal area causing higher drag and lower power to weight ratio of centrifugal compressors, axial flow compressors are gaining more popularity over the centrifugal compressors. Efficiency is probably the most important performance parameter for turbomachines. But there are various losses associated with turbomachines that tend to reduce the performance of turbomachines. Tip leakage loss plays a major role in reducing the performance because of less knowledge of flow field in the tip region. The performance of a compressor is sensitive to tip region geometry and

flow in that region, as it affects the flow over much of the blade span. The tip leakage loss thus would have a dominant effect on the performance of a compressor. Low aspect ratio compressors are gaining popularity over the large aspect ratio compressors because these compressors have higher loading levels, higher efficiency, better stability and vibrational characteristics (see Wennerstrom[1]). But the flow in low aspect ratio compressors is highly three dimensional, the loading on the blade is very high and relative tip clearance is large. So the tip clearance effects are more dominant.

Although very small tip clearances are desirable for improved performance and operating range, it is not always easy to maintain small clearances, because of reduced safety of rotor blades and increased manufacturing costs. Many active and passive means have been tried to reduce the deleterious effects of tip clearance flows. For example, active means such as air injection at the casing[2] and passive means such as recessed vane casing[3] have been successfully used to improve the pressure rise and operating range of axial flow compressors. These methods are quite expensive and are normally used in axial compressors for aircraft and industrial gas turbines. Kameier and Neise[4] reported improved pressure rise, increased operating range and reduced noise by using a simple technique, i.e. by placing a velcro tape in the clearance between the casing and the rotor blade of a commercial blower. This method is useful only when the clearance is sufficiently large. The present paper reports results of an experimental investigation, where improved performance and operating range of a low aspect ratio axial flow compressor are obtained by using a similar technique. In this technique, the turbulence generator (velcro tape) is placed upstream of the rotor leading edge. Thus this technique can be used even when the tip clearance is small.

2. EXPERIMENTAL FACILITY, INSTRUMENTATION AND PROCEDURE

The present investigation is carried out on the low aspect ratio axial flow compressor. A schematic layout of the test facility is shown in Fig. 1. The rotor tip diameter, d_t is 0.580 m and hub diameter is d_h of 0.450 m, giving a hub/tip ratio of 0.77. Further details are the facilities are given in Table 1. The rotor tip clearance is 1.5 mm giving a relative tip clearance of τ = 1.1%. Details of the rotor blades are given in Table 2. The volume flow rate of air through the rotor is measured using the calibrated inlet nozzle. The speed of the rotor is measured with a non-contact type electronic tachometer with an accuracy of 1 rpm. The casing has provision to mount traversing mechanisms at three axial locations S_1, S_2 and S_3, at the inlet and exit of the rotor and exit of stator respectively. Static pressure tappings are provided on the casing at inlet and exit of the rotor and exit of the stator. Turbulence generators are used in the experiment as a tripping device for the generation of turbulent boundary layers. A turbulence generator (TG) is pasted on the casing wall upstream of the rotor. A turbulence generator (TG) is made of an approximately 2 mm thick Velcro tape material of 1820 mm long and 25 mm width. Another turbulence generator (TG1) of the same material and length but 15 mm wide is pasted on the casing wall upstream of rotor 44 mm away from the leading edge of the rotor. The rotor exit flow using a pre-calibrated five hole probe. The non- nulling method of Treaster and Yocum[5] is used for calibrating and interpolating the measured data of five hole probe. A scanning box (Model FCO91-3) and micromanometer (Model FCO12), manufactured by M/s. Furness Control Ltd., UK, are used to measure the pressure sensed by the pressure probes. The scanning box contained 20 valves which are numbered sequentially. The pressures to be measured are connected to the numbered inputs. Pressure inputs are read in sequence by using the micromanometer. The micromanometer is a sensitive differential pressure measuring unit, capable of reading air pressures from 0.01 mm to 200 mm WG. It would respond to pressure inputs up to 50 Hz. But the time constant potentiometer can be used to average the pressure fluctuations. The accuracy of the measured pressure is within $\pm$ 0.01 mm WG.

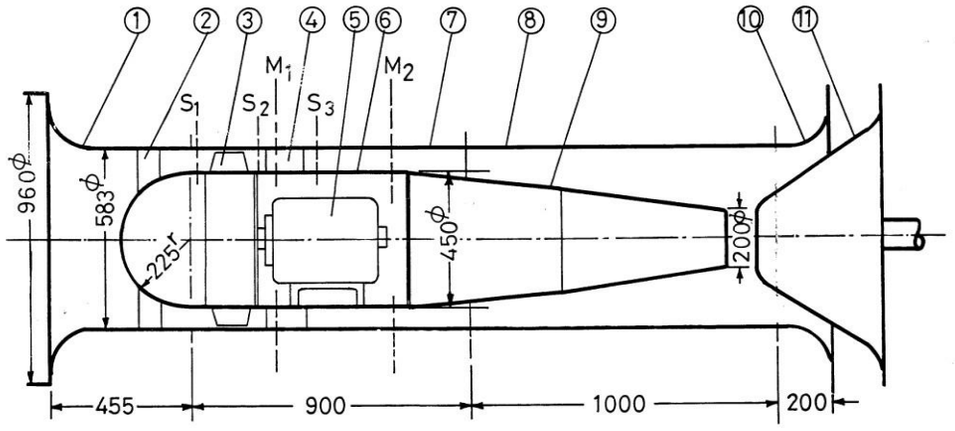

All Dimensions in Millimeters

Figure.1 - 1. Inlet Nozzle2. Radial Supports for Hub Nose Cone 3. Rotor 4. Stator 5. A.C. Motor 6. Motor Housing 7. Casing 8. Exit Duct 9. Conical Hub 10. Exit Nozzle 11. Throttle Cone M1 and M2: Location of Stay Rods for Motor Housing S1, S2 and S3: Traverse Stations for Probes.

3. RESULTS AND DISCUSSION

The results of the present experimental investigations are presented and interpreted in the following sections. First the rotor performance, in terms of static pressure coefficient across the rotor tip, derived from casing wall static pressures measured before and after the rotor for the four configurations is presented. The results at the rotor exit are presented later in the form of total pressure coefficient, static pressure coefficient, velocity and flow angle. The results are presented for four configurations including basic configuration and at five flow coefficients, viz. ϕ = 0.65 (above design flow coefficient), ϕ = 0.55 (design flow coefficient), ϕ = 0.48 (below design flow coefficient), ϕ = 0.42 (stall flow coefficient) and ϕ = 0.35 . The four configurations studied are (i) rotor without passive means, tip clearance τ = 1.1% (ii) rotor with partial shrouds (PS), tip clearance τ =1.1%, (ii) rotor with partial shrouds (PS) and turbulence generator (TG) upstream of the rotor leading edge, tip clearance τ =1.1% and (iv) rotor with partial shrouds (PS) and turbulence generator (TG1) 44 mm upstream of the rotor leading edge, tip clearance τ = 1.1%. The velocities are non-dimensionalised by imaginary blade speed based on the casing radius i.e. U_C. The total and static pressures are non-dimensionalised by the dynamic head derived from U_C. These non-dimensional values are presented against the percent span from hub.

3. PERFORMANCE CHARACTERISTICS

The performance characteristics of the low aspect ratio axial flow compressor rotor for four configurations are shown in Fig. 2. The abscissa of this figure represents flow coefficient, whereas, ordinate represents the static pressure rise coefficient across the rotor at the casing. It can be seen that Configuration 4 (rotor with PS and TG1) shows increased static pressure rise across the rotor at casing compared to other configurations. The reason is that TG1 energises the casing wall boundary layer. Stall occurs at □□= 0.44, compared to Configuration 1 (Basic configuration), for which stall occurs at □□= 0.464. Also it is observed that, when the turbulence generator (TG) is placed just upstream of the rotor leading edge (Configuration 3), static pressure rise across the rotor tip is reduced drastically. Stall occurs at a higher flow coefficient of 0.475. The most probable reason for this may be due to the large disturbances caused by the TG right at the rotor leading edge. It is also observed that with PS, stall occurs at a higher flow coefficient. The values of stall flow coefficient for the four configurations are given in Table 3.

4. ROTOR EXIT FLOW MEASUREMENTS

***Total pressure coefficient*:** ζ_{02}: The distribution of total pressure coefficient at the rotor exit for four configurations and five flow coefficients is shown in Fig. 2. From the figure it is clearly seen that, the free vortex design of the rotor is confirmed by the total pressure distribution at ϕ = 0.55, which is almost constant outside the annulus wall boundary layers. Figure 4 clearly shows that for ϕ= 0.64, 0.48 and 0.42, there is a definite increase in total pressure over a large radial extent for the rotor with the configuration of PS and TG1 compared to configurations of rotor with PS and with PS and TG. But for ϕ= 0.36 rotor with PS show more total pressure rise as compared to rotor with PS and TG1 but with reduced stable operating range as stall occurs at higher flow coefficients, whereas, at design flow coefficient ϕ = 0.55 both these configurations show almost same total pressure rise. However, it is to be noted that for all flow coefficients basic configuration of rotor shows more total pressure rise compared to other configurations. Although turbulence generator (TG1) placed upstream of the rotor leading edge may be beneficial for the rotor performance, the benefit may not be sufficient to overcome the detrimental effects of partial shrouds. The vortices generated by turbulence generator TG1 which is pasted on the casing wall upstream the rotor leading edge, the casing wall boundary layer gets energised. Due to this, separation of boundary layer is delayed and hence losses are less. Consequently, better stable operating range is achieved. Similar benefits are observed by Wennerstrom[6], when casing vortex generators are used in a transonic axial compressor. The casing vortex generators used by him are of 1.5 mm height and are spaced at 6.5 mm placed at 36 mm from the rotor leading edge. The main purposes of vortex generators were to maintain sufficient energy in the casing boundary layer to discourage separation on the casing due to shock boundary layer interaction or loading.

Static pressure coefficient, ζ_{S2}: The distribution of static pressure coefficient for the five flow coefficients and four configurations, at the rotor exit is shown in Fig.2. From figure it is seen that for basic configuration as well as for other configurations static pressure rise remains almost constant. For ϕ = 0.64, Configuration 2 of rotor i.e. rotor with partial shrouds only (PS) shows large fluctuations in static pressure from hub to tip due to use of partial shrouds. Similarly with configuration of rotor with PS and TG1, static pressure is again fluctuating due to turbulence generator. But static pressure coefficient for this configuration is less than that for configuration only with PS. This is because of suppression of boundary layer separation due to vortices generated by TG1.

Careful study of this figure shows that static pressure coefficient is more for basic configuration. This is due to leakage flow acts in opposite direction of secondary flows, the static pressure rise is not high even though for these flow coefficients (except for ϕ = 0.48) total pressure is high. For ϕ= 0.42, total pressure is more, therefore static pressure is expected to be more for Configuration 4 (rotor with PS and TG1) compared to Configuration 2 (rotor with PS only) but due to generation of turbulent boundary layers by TG1, static pressure rise reduced.

Absolute velocity, C_2: The span wise distribution of absolute velocity for the five flow coefficients and four configurations is shown in Fig.2. It can be seen from the figure that the absolute velocity almost remains constant at design flow coefficient and above the design flow coefficient (ϕ = 0.64 and 0.55). Also it is observed that these flow coefficients show the same

absolute velocity for shrouded cases. Careful study of this figure shows that basic configuration give lower absolute velocity for flow coefficient at, above and just below design flow coefficient. This lower absolute velocity is due to leakage vortex in the flow field which mixes with the main flow at the exit resulting in lower values of velocities, whereas at lower flow coefficient basic configuration of rotor gives higher velocity and higher absolute velocity; means this higher leaving kinetic energy which is not a desirable characteristic.

Absolute flow angle, α_2: The span wise variation of absolute flow angle for the five flow coefficient and for the four configurations at the rotor exit is shown in Fig.2. The angles shown are with respect to tangential direction. For ϕ = 0.64, 0.55 and 0.36, from Fig. 7, it is clear that for Configuration 4 (rotor with PS and TG1) lower absolute flow angles have been observed for the most of the span. With almost same axial velocity and decrease in absolute flow angle means increase in tangential velocity, which in turn causes more losses. But lower absolute flow angle for the same axial velocity indicates higher absolute velocity with Configuration 4 (rotor with PS and TG1) compared to Configuration 2 (rotor with PS only) and thereby higher total pressure. For ϕ = 0.55, the absolute flow angle falls down at 82.5% of span wise distance from hub, for rotor with PS and TG1. So the incidence angle at stator inlet for the configuration is higher.

5. MASS AVERAGED FLOW PARAMETERS

Figure.2. shows the variation of mass averaged values of total pressure rise efficient and static pressure rise coefficient with flow coefficient. This figure clearly shows improvement in ψ total pressure rise efficient and static pressure rise coefficient with flow coefficient for rotor (with MPS and TG1) compared to rotor (with PS only) and rotor (with PS and TG). Due to vortices generated by TG1 upstream of rotor, casing wall boundary layer is energised, which cause delay in boundary layer separation consequently losses are reduced. Configuration 4 (rotor with PS and TG1) shows improved pressure rise than that of Configurations 2 and 3. But static pressure rise for this configuration in tip region is slightly less than that of Configuration 3. This configuration shows early stalling compared to Configuration 4. This early stalling may be due to boundary layer separation due to high adverse pressure gradient at this flow coefficient.

6. CONCLUSIONS

1. From the performance of rotor determined from the wall static pressures measured on the casing before and after the rotor tip, Configuration 4 (rotor with PS and TG1) stalls at a lower flow coefficient compared to other configurations. Also the static pressure rise coefficient is slightly higher compared to that for other configurations. Configuration 2 (rotor with PS) and Configuration 3 (rotor with PS and TG) gave poor performance, i.e. reduced operating range and reduced static pressure rise coefficient over the entire operating range.
2. Turbulence generator (TG) which was placed at leading edge of the rotor caused early stalling. This is avoided by using turbulence generator (TG1) upstream of rotor away from the rotor leading edge.
3. Turbulence generator (TG1) causes the casing wall boundary layer to get energized which in turn causes delay in boundary layer separation. Hence losses are less and better stable operating range is achieved. Although, measurements at the rotor inlet cannot taken for Configuration 4, due to the disturbed flow because of TG1, it is believed that the boundary layer at the rotor is turbulent even at near stall flow coefficient, = 0.42 and below.

4. The mass averaged total pressure rise coefficient and static pressure rise coefficient show improved for Configuration 4 (rotor with PS and TG1) compared to Configuration 3 (rotor with PS and TG). However the basic configuration shows higher values. For a proper comparison, only the performances of Configurations 3 and 4 must be compared, as both would include the detrimental effects of modified partial shrouds.

REFERENCES

[1] Q. H. Nagpurwala, S. P. Ramesh and S. A. Guruprasad, —Suppression of Rotating Stall in an Axial Flow Compressor through Air Jets||, Proc. of the Seventh Asian Congress on Fluid Mechanics, pp. 489-492, Dec. 8-12, Chennai, India.

[2] B. Roy and L. Agrawal, -Casing Boundary Layer Control by Recessed Vaned Casing for a Twin Rotor Contra-Rotating Axial Flow Fan Unit||, ASME Paper 94-GT-476, 1994.

[3] F. Kameier and W. Neise, —Reduction of Tip Clearance Loss and Tip Clearance Noise in Axial Flow Machines||, AGARD CP-569, 1995.

[4] M. Inoue and M. Kuroumaru, —Structure of Tip Clearance Flow in an Isolated Axial Compressor Rotor,|| ASME paper number 88-GT-251, 1988.

[5] B. Lakshminarayana, M. Zaccaria, and B. Marathe, -The Structure of Tip Clearance Flow in Axial Flow Compressors,|| ASME Journal of Turbomachinery, Vol. 117, No. 3, pp. 336–347, 1995.

[6] R. E. Peacock, -Turbomachinery tip gap aerodynamics,‖ in Proceedings of the 9th International Symposium on Air Breathing Engines, pp. 549–559, Athens, Greece, September 1989.

[7] D. C. Wisler and B. F. Beacher, —Improved Compressor Performance Using Recessed Clearance (Trenches),|| AIAA Journal of Propulsion and Power, vol. 5, no. 4, pp. 469–475, 1989.

[8] S. D. Hill, R. L. Elder, and A. B. McKenzie, -Application of Casing Treatment to an Industrial Axial-Flow Fan,|| Proceedings of the Institution of Mechanical Engineers, Part A, Vol. 212, No. 4, pp. 225–233, 1998.

[9] H. Khaleghi and J. A. Teixeira, —Numerical Study of Discrete Tip Injection in a Transonic Axial Compressor,|| in Proceedings of the ASME Turbo Expo Turbine Technical Conference, no. GT2010-23608, pp. 525–535, Glasgow, UK, June 2010.

[10] J. Giridhar, R. C. Murray, K. Essenhigh et al., —Control of Tip-Clearance Flow in a Low Speed Axial Compressor Rotor with Plasma Actuation,|| in Proceedings of the ASME Turbo Expo Turbine Technical Conference, no. GT2010-22345, pp. 161–172, Glas-gow, UK, June 2010.

[11] M. Ishida, H. Ueki, and Y. Senoo, -Effect of Blade Tip Configuration on Tip Clearance Loss of a Centrifugal Impeller,|| ASME Journal of Turbomachinery, vol. 112, no. 1, pp. 14–18, 1990.

[12] A. Corsini, F. Rispoli, and A. G. Sheard, —Shaping of Tip End-Plate to Control Leakage Vortex Swirl in Axial Flow Fans,|| ASME Journal of Turbomachinery, vol. 132, no. 3, pp. 1–9, 2010.

[13] A. Akturk and C. Camci, —Axial Flow Fan Tip Leakage Flow Control Using Tip Platform Extensions,|| ASME Journal of Fluids Engineering, Vol. 132, No. 5, pp. 0511091–05110910, 2010.

[14] A. Akturk and C. Camci, —Tip Clearance Investigation of a Ducted Fan used in VTOL UAVs, part 1: Baseline Experiments and Computational Validation,|| in Proceedings of the ASME Turbo Expo Turbine Technical Conference, no. GT2011-46356, Vancouver, Canada, June 2011.

[15] A. Akturk and C. Camci, -Tip Clearance Investigation of a Ducted Fan Used in VTOL UAVs, part 2: Novel Treatments Via Computational Design and Their Experimental Validation||,

Proceedings of the ASME Turbo Expo Turbine Technical Conference, no. GT2011-46359, Vancouver, Canada, June 2011.

[16] A. J. Wennerstrom, —Low Aspect Ratio Axial Flow Compressors: Why and What it Means,|| ASME Journal of Turbomachinery, Vol. 111, No. 4, pp. 357–365, 1989.

[17] H. H. Brunn, A. Fitouri, and M. K. Khan, -The use of multi-position single yawed hot wire probe for measurements in swirling flow,|| ASME FED 167, Thermal Anemometry, pp 57-65, 1993.

APPENDIX

Table 1 Details of the Low Aspect Ratio Axial Flow Compressor

Design volume flow, V	= 3.5 m^3/s	Speed, n	= 1450 rpm
Specific work, W	= 650 m^2/s^2	Free vortex design	
Rotor hub diameter, d_h	= 450 mm	Rotor tip diameter, d_t	= 580 mm
Number of rotor blades, Z_R	= 14	NACA 0008 type FRP rotor blades	
Number of stator blades, Z_S	= 13	Circular arc sheet metal stator blades	
Rotor aspect ratio, AR_R	= 0.5	Stator aspect ratio, AR_S = 0.47	

Table 2 Details of Rotor and Stator Blades

		Rotor Blades					Stator Blades				
Sl. No.	**D mm**	**1b Deg.**	**2b Deg.**	**Deg.**	**s/Ch**	**Ch_R mm**	**2b Deg.**	**3b Deg.**	**s/Ch**	**Ch_S mm**	**R_S mm**
1	450	35.2	59.5	55.0	0.743	136	54	100	0.750	145	185
2	477	33.6	55.7	52.9	0.789	136	54	100	0.795	145	185
3	505	32.2	52.3	48.8	0.834	136	54	100	0.842	145	185
4	532	30.8	49.1	45.9	0.878	136	54	100	0.887	145	185
5	560	29.5	46.2	43.3	0.924	136	54	100	0.934	145	185
6	580	28.4	43.5	40.7	0.962	136	54	100	0.972	145	185

Table 3 Stall Flow Coefficient for Different Configurations

Configuration No.	Config. 1	Config. 2	Config. 3	Config. 4
stall ϕ	0.464	0.475	0.475	0.440

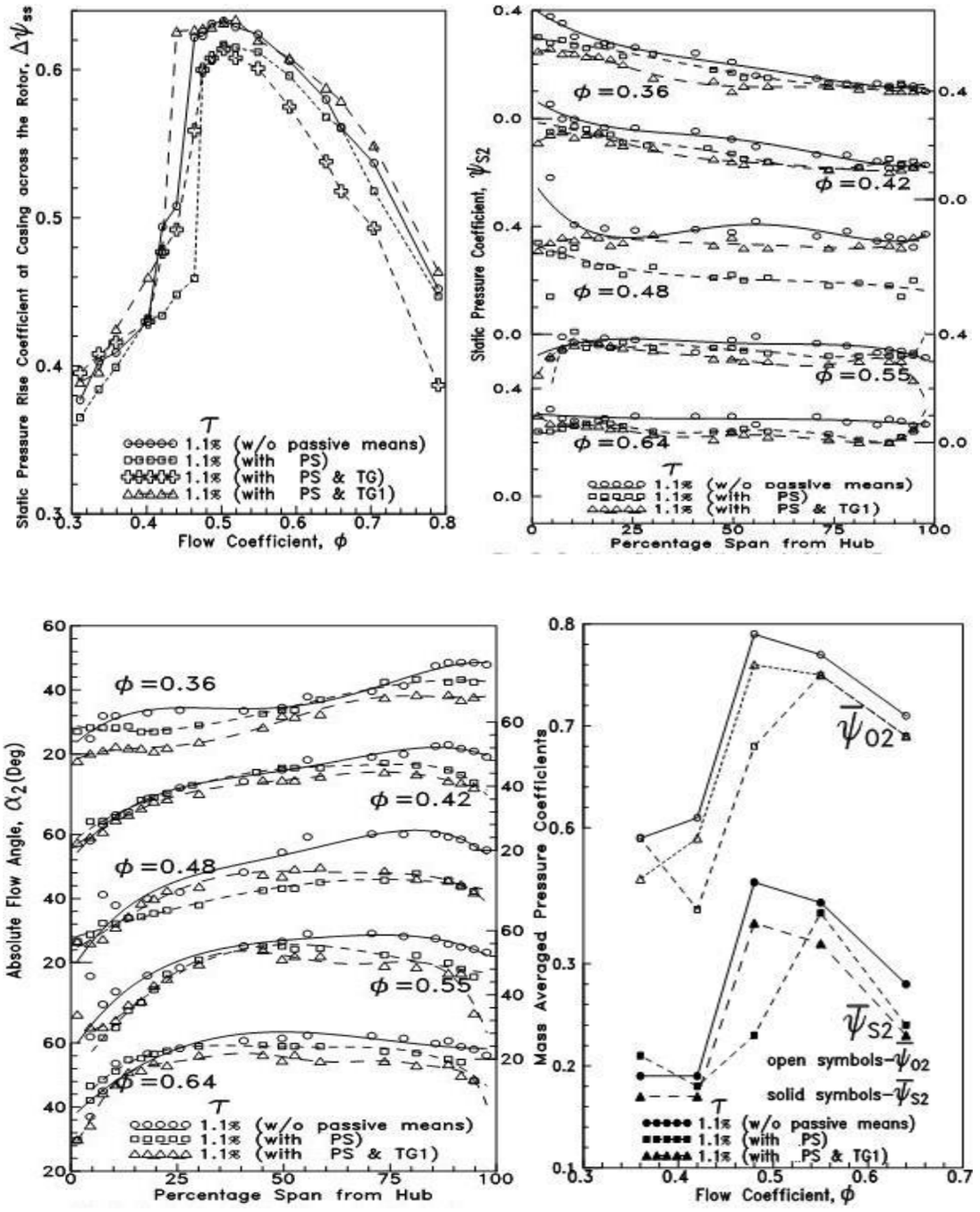
Static Pressure Rise Coefficient at Casing across the Rotor, $\Delta\psi_{ss}$
Flow Coefficient, ϕ
T
1.1% (w/o passive means)
1.1% (with PS)
1.1% (with PS & TG)
1.1% (with PS & TG1)
Static Pressure Coefficient, ψ_{S2}
ϕ =0.36
ϕ =0.42
ϕ =0.48
ϕ =0.55
ϕ =0.64
Percentage Span from Hub
Absolute Flow Angle, α_2(Deg)
Mass Averaged Pressure Coefficients
$\overline{\psi}_{02}$
$\overline{\psi}_{S2}$
open symbols-$\overline{\psi}_{02}$
solid symbols-$\overline{\psi}_{S2}$

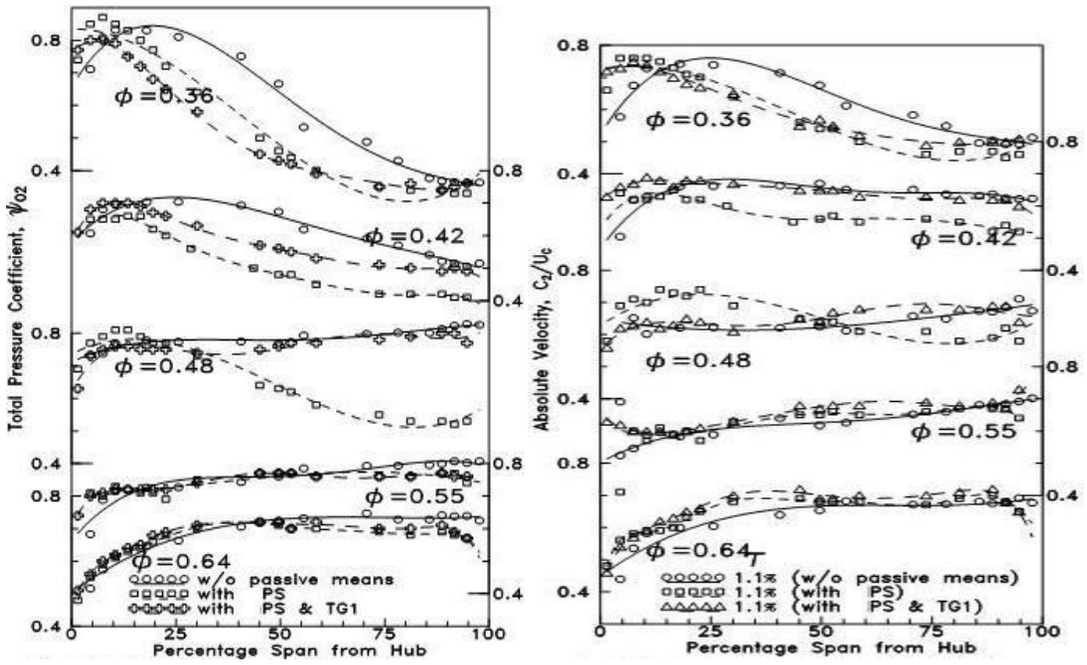

Fig.2 Performance characteristics of the low aspect ratio axial flow compressor rotor for four configurations

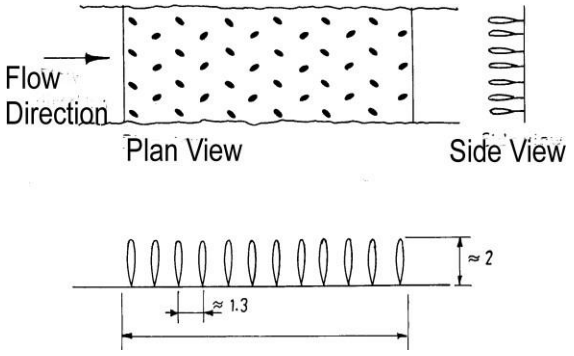

Figure.3 - 25 mm for TG and 15 mm for TG1
Turbulence Generator

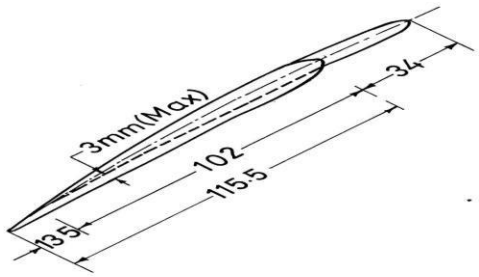

Figure 4 Partial Shroud

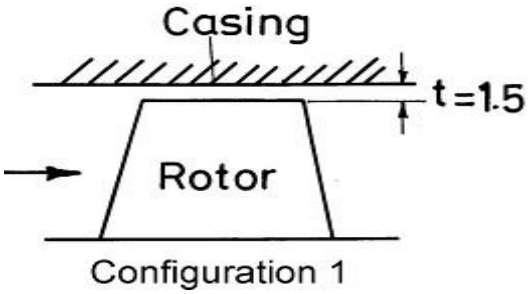

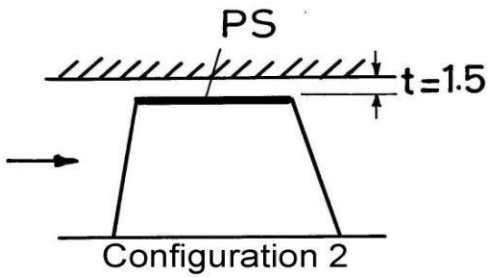

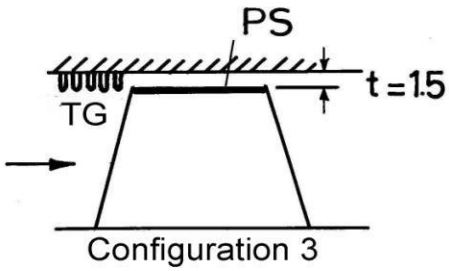

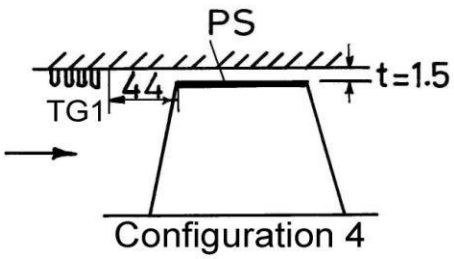

Configurations Tested